Improvement of thermal management of composites forming process tooling using lattice structures

Matthis Balthazar, Nicolas Baudin, Jérôme Soto, Denis Edelin, Sébastien Guéroult, Vincent Sobotka

Improvement of thermal management of composites forming process tooling using lattice structures

Matthis Balthazar[1,2], Nicolas Baudin[2], Jérôme Soto[2,3], Denis Edelin[2,3], Sébastien Guéroult[1], Vincent Sobotka[2*]

[1]Institut de Recherche Technologique Jules Verne, 1 Mail des 20 000 Lieues, Bouguenais, 44340, France.

[2]Nantes Université, CNRS, Laboratoire de thermique et énergie de Nantes, LTeN, UMR 6607, La Chantrerie, rue Christian Pauc, Nantes, 44306 cedex 03, France.

[3]Icam school of engineering, Nantes Campus, 35 avenue du champ de manoeuvres, Carquefou, 44470, France.

*Corresponding author(s). E-mail(s): vincent.sobotka@univ-nantes.fr;

Abstract

Thermal management is crucial in composite part manufacturing, as it directly impacts final quality. Controlling tooling surface temperature is essential to minimize defects and achieve desired mechanical properties. This article explores the use of lattice structures with heat transfer fluid circulation to enhance heat exchange, ensuring composite part quality and improving manufacturing productivity and energy efficiency. These structures improve temperature uniformity, increase heating and cooling rates, and reduce thermal inertia without causing thermal marks, thus decreasing cycle time and energy consumption. A steady-state numerical study examines the impact of geometry and materials on the tooling thermal-hydraulic performance. Analysis of fluid flow and heat transfer highlights the impact of the lattice structure on fluid and heat transfer flows. The disturbance created by lattice structures is the main driving force behind improved heat transfer in the system studied. In the presented configuration i.e. water and high fluid flowrate, the performances do not depend strongly on the lattice structure material. Even if the lattice structures increase the pressure drop the system studied generates a higher performance than a conventional thermal management method. Following this numerical study, experimental work was carried out in the unsteady regime, providing a proof of concept. The results show an improvement in the uniformity of the temperature field at the tooling surface during transient phases compared with a conventional design using straight

channels. The use of lattice structures improves temperature uniformity at the tooling surface by over 50 %, and heating and cooling rates by 77 %. Finally, the possibility of locally controlling the temperature field by adjusting the porosity of the lattice structure is highlighted.

Keywords: Composite manufacturing, Forming, Lattice structure, Heat transfer, Thermal management, Thermal efficiency

1 Introduction

The use of composite materials continues to increase, particularly in the transport industry. Manufacturing of these components remains a real challenge as their quality depends on numerous parameters, among which one is crucial: thermal management during the manufacturing cycle. The composite materials forming requires a controlled supply and release of heat into the part to guarantee quality while allowing maximum productivity. Inadequate thermal management can result in various defects in the component, including warpage, shrinkage, thermal residual stresses, and sink marks [1, 2]. Moreover, productivity of the process depends largely on the cooling time of the molded part. For example, in the case of thermoforming or injection molding processes, more than 50 % of the cycle time is dedicated to part cooling [3, 4]. The efficiency of cooling systems directly impacts both productivity and energy consumption of the manufacturing process. To ensure an optimal heat transfer between the part being produced and the mold, it is essential to use well-designed cooling and heating systems. Traditionally, this is achieved by incorporating multiple straight channels in the mold core and cavity, through which a cooling fluid, generally water or oil, flows. This conventional method, although easy to implement, poses problems of adaptation to complex shapes and does not guarantee a homogeneous temperature field.

Thanks to advances in additive manufacturing (AM), new designs can be created, with far greater design freedom than with conventional machining. There are many AM processes [5], and various metal alloys such as stainless steels, titanium, nickel and aluminum alloys can be used in additive manufacturing [6]. Previously straight channels can now take more complex shapes, allowing them to conform to the shape of the part and freely manage the distribution of channels to achieve better thermal performance. The benefits of additive manufacturing open up new avenues in the design and evolution of heat exchangers, enabling shapes to be optimized, exchange surfaces to be improved, and porous structures to be created [7]. Conformal cooling emerge, where channels are designed to follow the shape of the part, aiming to enhance cooling time and temperature uniformity [8]. In literature, design and optimization of conformal cooling are the focus of many studies [3, 9–18]. Channel optimization can lead to complex shapes, as studied by Mercado Colmenero & al [19] for injection mold cooling, resulting in increased efficiency of the manufacturing process, reducing cycle time and increasing the quality of the parts produced. There are many optimization processes, manufacturing procedures and optimization parameters in the design of conformal channels to reduce cycle times and improve the quality of the final part [18].

Some studies concentrate on optimizing the shape of channel cross-sections to enhance performance. For instance, Chil-Chyuan Kuo et al. [20] demonstrate that using profiled conformal cooling channels (PCCC) decreases cooling time by 33.33% compared to circular channels, while also improving the uniformity of the temperature distribution on the mold surface. Neil Wilson & al [21] also studied the impact of the shape of the channel section produced by hybrid manufacturing, showing that triangular channels offer the best performance in terms of heat transfer compared with the others tested in the study. More complex channel networks have also been studied, Au and Yu developed the introduction of a conformal layer composed of multi-connected porous passageways for mold cooling to improve temperature distribution [22].

Although conformal cooling channels significantly enhance performance, their design is constrained by specific design rules. The distance d_2 in figure 1 between the channels and the mold surface is limited by two factors: the mechanical strength of the mold and the thermal non-uniformity of the cavity surface, known as thermal marking. Furthermore, the distance between the fluid and the tooling surface (d_1 and d_2) in the case of circular channels is not constant, leading to a non-uniform temperature field if the channels are placed too close to the surface in contact with the composite part, as shown with the isotherme line in the figure 2. The thermal response time is diretly constrained by this distance which induces high thermal inertia.

An alternative to conventional approaches is the use of a porous medium consisting of lattice structures in which a regulating fluid circulates. Lattice structures are a distinct type of porous material distinguished from foams by the ordered and repetitive arrangement of their unit cells. These porous structures can be integrated into the tooling closest to the surface ($d_3 < d_2$) because they provide sufficient structural reinforcement and prevent thermal marking through a sheet flow, as shown in figure 2. Additive manufacturing enables the creation of this type of complex architected 3D patterns thanks to its high design freedom [23, 24]. This type of structure provides good mechanical strength [25], which is necessary in forming processes where high pressure is applied when the mold is closed.

The mechanical performance and fatigue resistance of lattice structures manufactured by additive manufacturing depend on several key parameters. Among them, powder morphology, laser exposure strategy and power, laser scanning speed and layer thickness all influence the quality of SLM manufacturing results [26]. These manufacturing parameters impact surface roughness, which subsequently affects the mechanical strength and fatigue resistance of structures by generating local stress concentrations [27]. Consequently, it is crucial to carefully optimize these manufacturing parameters to ensure optimum performance of lattice structures.

Brooks and Bridgen [28] have numerically and experimentally studied the use of such structures for injection molds to improve heat transfer rates and minimize tool temperature variations. Lepoivre & al [29] have experimentally investigated the enhancement of heat transfer as a function of lattice structure porosity, for thermoplastic injection molding. Valentine & al [30] investigated the benefits of additive manufacturing for the production of composite forming tooling. They concluded that the tooling was highly responsive thermally, with heating rates up to 17% faster than

monolithic tools of similar mass. Alessio & al [31] have studied the use of additive manufacturing to create lighter and thermally efficient molds for the manufacture of expanded polymer parts traditionally using massive molds. The study shows a significant reduction in cycle times and energy consumption with molds manufactured by laser powder fusion. Yun & al. [32] have studied influence of porosity of lattice structure on heat transfers, pressure loss and mechanical resistance. This study showed that for a constant flow rate, reducing the porosity of the structure increases the heat transfer coefficient. Dixit & al [33] evaluated and numerically compared the thermal and hydraulic performance of six different geometries for laminar flow. As a result of their study, they concluded that the centered cubic shape offered the best ratio of thermal efficiency / pressure drop. The shape of the structure's ligaments also has an impact on fluid flow, and therefore on the heat exchanger's thermal efficiency. Liang & al [34] studied the influence of shape experimentally and numerically, comparing three types of ligament: circular, rectangular and elliptical for the same structure. They concluded that the shape with the best performance is the circular one in terms of its ratio of thermal performance to pressure drop. Fuller & al [35] experimentally investigated the influence of the thermal conductivity of the porous structure material on overall heat transfer by comparing two foams with similar porosities: one made of FeCrAlY alloy and another with around 20 times higher thermal conductivity made of copper. For an equivalent heat transfer fluid (air) and Reynolds number, they obtained heat transfer coefficients 2 to 3 times higher for the more conductive copper foam.

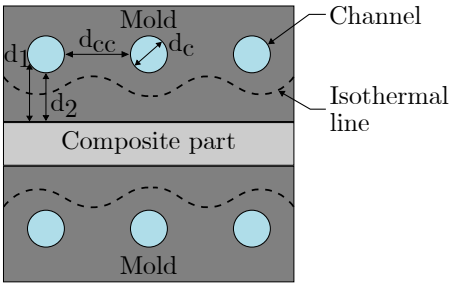

Fig. 1: Diagram of the conventional cooling system

Despite numerous studies on the use of lattice structures in heat transfer, analysis of the influence of structure geometry and material in the case of turbulent heat transfer fluid flow for application in composite tooling is still lacking. One of the objective of the study is therefore to determine which parameters influence the thermal-hydraulic performance of the tooling. Analysis of the evolution of the temperature field at the mold surface under transient conditions, as is the case in injection molding or thermoforming, has not been studied either. The use of porosity variation in the lattice structure to intentionally generate a change in the temperature field at the tool surface should also be investigated.

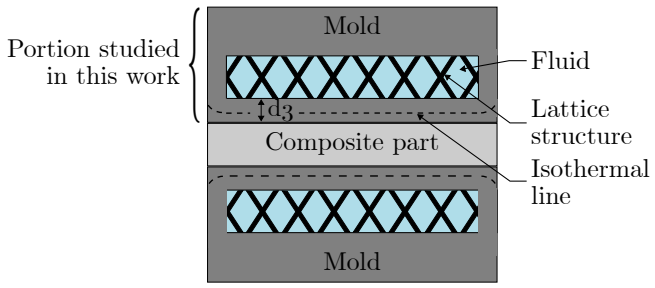

Fig. 2: Diagram of the system studied in this work

Based on these results, the first objective of this research paper is to evaluate the influence of the geometry (cubic geometry) of the lattice structure on the thermo-hydraulic performance of the system studied. The influence of the thermal conductivity of the lattice structure material on heat transfer within the tooling and on thermal efficiency is also analyzed. To achieve this objective, a steady-state numerical study coupling turbulent water flow and heat transfer is carried out using several configurations. This study enables local analysis of both heat transfer and fluid flow inside the lattice structure. This results led to the selection of the geometry offering the best thermo-hydraulic performance among those tested.

The second objective of this work is a transient thermal analysis of the system. To complete the steady-state analysis, and given the numerical cost involved, the unsteady state in which heating and cooling cycles are carried out as in an industrial process is studied experimentally. The main objective of this experimental part is to analyze the heating and cooling rates at the tooling surface and the homogeneity of the temperature field during transient phases. Finally, the possibility of controlling locally the temperature field at the tooling surface by adjusting the porosity of the lattice structure is investigated. This experimental study provides proof of concept and demonstrates the advantages in terms of efficiency of using additive manufacturing and this type of structure in composite forming tools used in thermoforming or injection molding, for example.

2 Lattice cell architectures

Lattice cell-topologies investigated in this study are body-centered-cubic (BCC) and face-centered-cubic (FCC) as shown in figure 3 with cylindrical ligaments. The "Z" corresponds to one additional ligament and the "Z+" to two additional ones. Z-ligments provide better compressive strength, as shown in the work of Leary & al [36]. Cubic geometries are commonly used for heat exchanger applications [28, 29, 32, 33]. Cubic geometries were chosen for several reasons. As shown by the work of Maconachie & al [26], BCCZ and FCCZ geometries offer good compressive strength properties for a given relative density. The choice of geometries for the structures studied is also based on the constraints of additive manufacturing techniques. These cubic geometries can be easily produced using additive manufacturing techniques, an essential parameter

for industrial application. The proposed geometries can be realized without the need for additional support, using a maximum strand angle of 45° to the vertical.

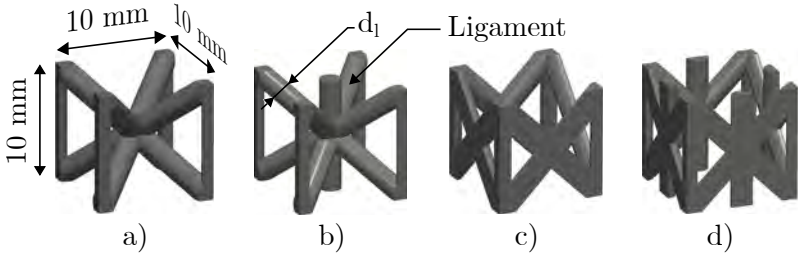

Fig. 3: Unit cells geometries. a) BCCZ, b) BCCZ+, c) FCCZ, d) FCCZ+

Each unit cell has a fixed overall dimension of 10 mm × 10 mm × 10 mm. Porosity ε (eq. 1) is fixed at 0.8 by adjusting ligament diameter d_l between each cell-topology.

$$\varepsilon = \frac{V_{void}}{V_{total}} \tag{1}$$

Where V_{void} is the volume of void-space and V_{total} is the total cell volume. Cells characteristics are summarized in table 1. As the porosity is the same for each geometry, the volume of fluid is also the same. However, the contact surface with the fluid is not the same for each geometry, which can potentially modify heat exchange. A_c is this area of the contact surface of the unit cells with the fluid called the wetted area.

Table 1: Characteristics of used unit cells

	d_l $(10^{-3}\ m)$	A_c $(10^{-6}\ m^2)$
BCCZ	2.00	355
BCCZ+	1.90	377
FCCZ	2.25	319
FCCZ+	1.96	363

In the rest of the study, these unit cells are joined end-to-end to create a straight channel. The straight-channel configuration is used for both numerical and experimental works. The straight channel is used in the study, but it is possible with this technology to realize a flow sheet.

3 Experimental setups

The aims of the experimental setups are to analyze the temperature field at the surface of the system in steady and transient states, and to study the pressure drop generated by the lattice structure. The steady-state setup configuration is used to validate the

numerical results by comparing numerical temperature field and pressure drop with the experimental results. Then, a study in unsteady-state is realized to carry out heating and cooling cycles to get closer to industrial use. The objectives are to analyze heating and cooling rates on the tooling surface and homogeneity of the temperature field on the same surface during transient phases. In both cases, the fluid used is water, as it is commonly used for thermal regulation.

3.1 Steady-state setup

To validate the results of the numerical model, an experimental bench is developed allowing the circulation of water inside a 20 cm long by 2 cm wide lattice channel while applying a constant heat flux on its top surface. The water circulates through the test section at T_{in} = 20 $°C$ and 2 $L.min^{-1}$ which is the permissible flow rate of the thermostat used. Lattice structure integrated into the channel is made of polymer and realized in the laboratory by stereolithography (properties in table 3). Figure 4 presents schematically the experimental setup.

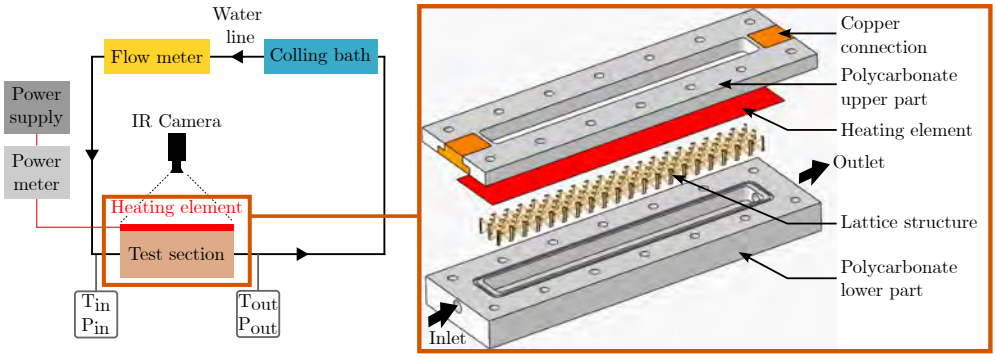

Fig. 4: Schematic of the experimental setup in steady state configuration

A homogeneous heat flux density of ϕ_{exp} = 23 $kW.m^{-2}$ is applied by Joule effect with an electrical resistance made of a sheet of stainless steel (thickness : $e_{stainless,steel,sheet}$ = 10 μm). To avoid electrical problems, the stainless steel sheet is electrically insulated on its two faces by two polyimide adhesive films of $e_{polyimide,film}$ = 49 μm thickness and a thermal conductivity $\lambda_{polyimide,film}$ = 0.17 $W.m^{-1}.K^{-1}$. The electrical resistance is presented schematically in figure 5.

Physical contact between the heating element and the lattice structure is obtained by bonding with cyanoacrylate glue. Temperature field at the top of the electrical resistance is measured with an infrared camera FLIR SC7000. A black paint "Kontakt Chemie GRAPHIT 33" of known emissivity (0.84, experimentally measured) is applied to the visualized surface. The fluid inlet and outlet temperatures are measured using two K-type thermocouples. Pressure drop between inlet and outlet of the test section is measured by two pressure sensors "Gems 3500B". For this part, only two cells are observed with the infrared camera to achieve a good resolution of 124 pixels by 69 pixels.

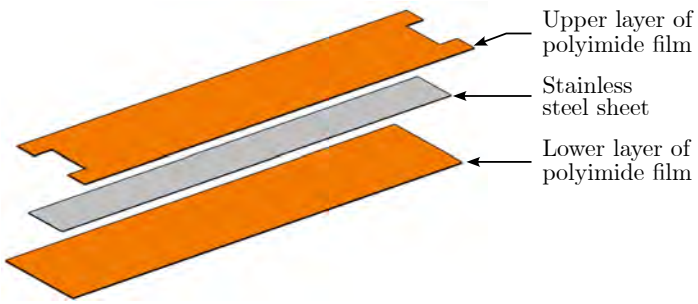

Fig. 5: Schematic of the heating element

3.2 Unsteady-state setup

The objective of the unsteady setup is to carry out heating and cooling cycles. These latters are obtained by alternating cold and hot water circulation in the test section. Hot and cold water temperatures are controlled by a cooling bath at $T_c = 20\ ^\circ C$ and a heating one at $T_h = 70\ ^\circ C$. The cold and hot loops are controlled by solenoid valves (SV) to have circulation cycles of cold water during 60 seconds and hot one during 60 seconds. On the top of the channel the heating element used in the steady-state setup is replaced by a stainless-steel plate of 5 mm thickness representing the tooling skin. The upper surface of this plate represents the molding cavity surface in contact with the composite part. This surface referred to as "tooling surface" (shown in red in figure 6) is observed by the infrared camera during the cycles, to analyze the evolution of temperature over time. Channel dimensions are the same as those used for the steady-state configuration. The lattice structure can be integrated in or removed from the channel to compare the temperature evolution of the tooling surface between these two configurations. The same black paint is applied on the observed surface as for the steady-state measurement. The experimental set-up is depicted in figure 6.

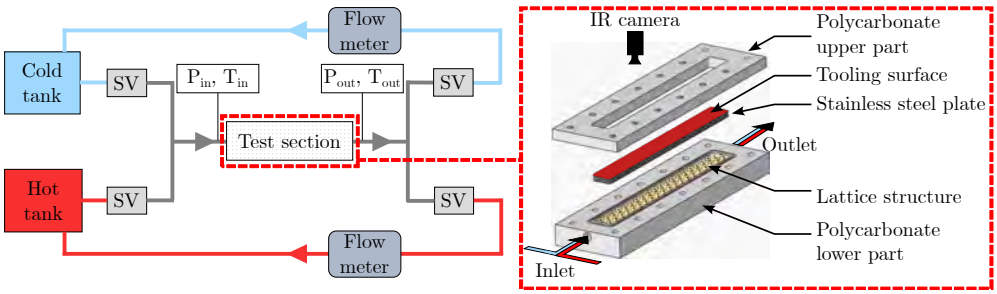

Fig. 6: Schematic of the experimental setup in unsteady state configuration

Figure 7 shows the lattice structure produced by additive manufacturing in polymer, and two cross-sections of the setup along the length of the channel representing the two configurations compared in this work.

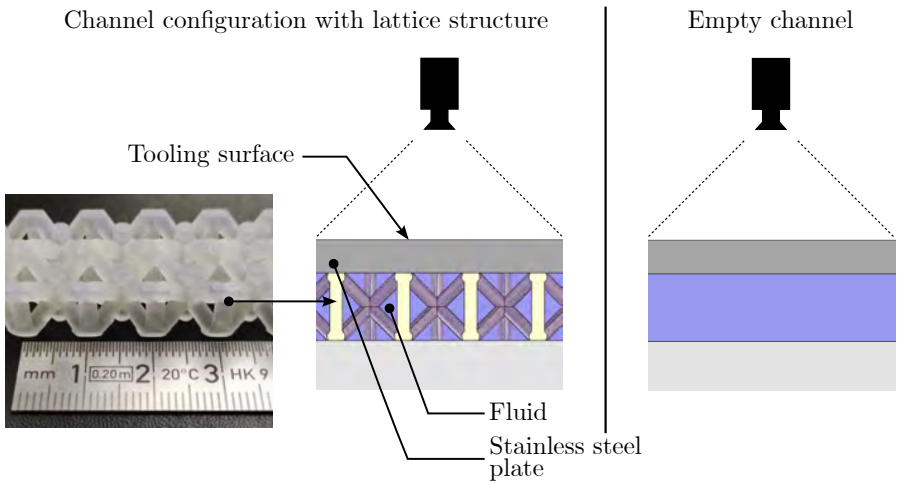

Fig. 7: Lattice structure produced by additive manufacturing and cross-section of the setup

4 Computational model

In order to quantify the efficiency of the selected structures, a numerical model is defined. This model aims to analyze the heat exchange and the fluid flow in a system composed of a channel containing a series of elementary cells through which the fluid circulates. The numerical solving of the fluid flow coupled with heat transfer is performed using the finite volume method with the software Ansys Fluent®. The governing equations of continuity, momentum and energy in the fluid domain are solved. The pressure-velocity coupling is implemented by coupled algorithm which ensures stable convergence in this case. The study is conducted in three dimensions, under steady-state conditions, and several assumptions are made: constant thermophysical properties, incompressible and single-phase flow, steady-state flow and no gravity effect.

4.1 Computational domain and boundary conditions

Figure 8 shows the computational domain used, and table 2 shows the values of the operating conditions for the simulation. The number of lattice cells used is sufficient to have study cells outside zone where the fluid flow and heat transfer are affected by the inlet in the lattice structure and outlet. A constant velocity and temperature are applied to the fluid at the inlet. The inlet velocity corresponds to a flow rate of 6 $L.min^{-1}$. A homogeneous and constant heat flux is applied to the upper part of the system on the tooling surface. This heat flux is representative of the one supplied by a composite part during its cooling, and is chosen to obtain a surface temperature around 100 $^{\circ}C$.

To ensure a hydrodynamically developed flow, an extended inlet of 100 mm long is included. Additionally, to avoid convergence issues caused by back pressure, an

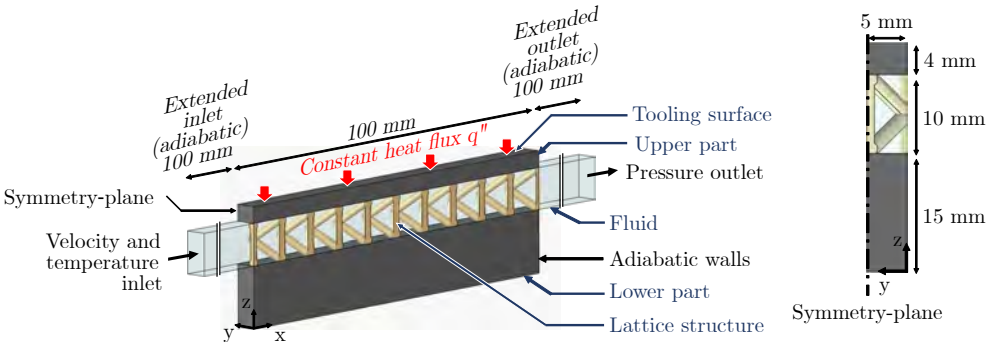

Fig. 8: Computational domain and boundary conditions

Table 2: Boundary conditions for simulation

Parameter	Value
Inlet temperature T_{in}	26.85 $^{\circ}C$
Inlet velocity v_{in}	1 $m.s^{-1}$
Outlet relative pressure P_{out}	0 Pa
Heat flux density q"	250 000 $W.m^{-2}$
No-slip condition at the fluid solid interface	-

extended outlet section is implemented. Taking advantage of the symmetry of lattice samples, only half of the configuration is simulated. The fluid used is water, lower and upper parts are considered to be made of 316L stainless steel. The lattice structure is either stainless steel or polymer in order to analyzed impact of the material of the structure on heat transfer. Material properties used are described in table 3.

Table 3: Material properties

Material	ρ $(kg.m^{-3})$	λ $(W.m^{-1}.K^{-1})$	Cp $(J.kg^{-1}.K^{-1})$	μ $(kg.m^{-1}.s^{-1})$
Water	998	0.60	4 182	0.001
Stainless steel	8 030	16.30	502	-
Polymer	1 400	0.22	1 200	-

Grids are generated in solid and fluid domains using Ansys Mesh®. Figure 9 shows the mesh characteristic with triangular prismatic elements in the inflation layer and tetrahedral elements on the rest of the domain. About twenty inflation layers are generated near the walls of the computational domain with a thickness of the first layer to ensure that value of the dimensionless wall distance y^+ was around unity.

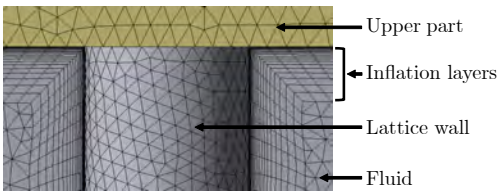

Fig. 9: Meshing of the domain

4.2 Turbulence model

Reynolds number is 9 980 at the inlet of the domain when $v_{in} = 1\ m.s^{-1}$, therefore a turbulence model is used. A low-Reynolds model is used, benefiting from the capability to resolve the near-wall flow by integrating the turbulent kinetic energy and dissipation rate equations up to the wall. The Shear Stress Transport k-ω (SST k-ω) turbulence model is used, providing accurate results for both laminar and turbulent flows as shown in [34, 37], and considering near-wall and wall-shear boundary conditions. Several studies used the SST k-ω turbulence model to accurately describe the flow of fluids in porous media coupled with heat transfer, exhibiting strong agreement with experimental results [32, 34, 37, 38].

4.3 Grid independence study

In this study, a pressure-based algorithm is employed in conjunction with a coupled solver scheme. Convergence of the simulation is considered obtained when residual of each conserved variables values fall below 10^{-4} for continuity, x-velocity, y-velocity, z-velocity, the turbulent energy kinetic k, turbulent dissipation rate omega, and 10^{-6} for energy. Throughout the iterative process, variables of interest, including average temperature of the tooling surface ($T_{avg,ts}$), inlet pressure (P_{in}), and maximum fluid velocity (v_{max}), are monitored to verify the stability of the simulation.

For the grid independence test, three grid schemes were generated. The number of elements is refined following the procedure grid refinement by calculating factor r eq. 2 [39]:

$$r = \left[\frac{N_{grid,n}}{N_{grid,n-1}}\right]^{1/3} \tag{2}$$

With N the number of elements of the mesh, n the finer mesh and n-1, the coarser mesh. The value of r must be greater than 1.3 based on experience [39]. For this mesh convergence, two variables of interest are compared: the convective heat transfer coefficient h_{eq} and the pressure drop ΔP between the inlet and the outlet of the fluid. Using these two variables allows to focus on heat transfer through h_{eq} (eq. 3) and fluid flow through ΔP.

$$h_{eq} = \frac{q"}{T_{avg,ls,up} - T_{avg,fl}} \tag{3}$$

Where $T_{avg,ls,up}$ is the average temperature of the lower side of the upper part in contact with the fluid and the lattice structure represented in green in figure 10.

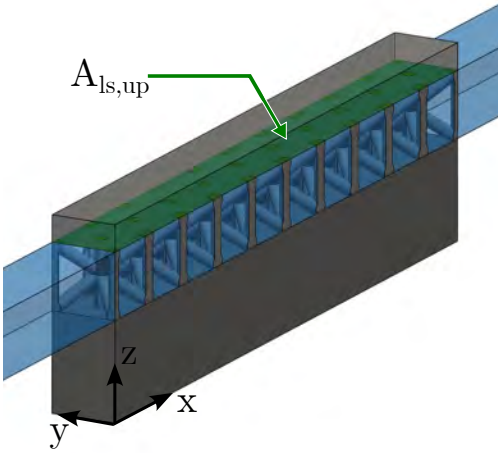

Fig. 10: Contact surface between the upper part, the fluid and the lattice structure : $A_{avg,ls,up}$

$T_{avg,fl}$ is the average fluid temperature defined as:

$$T_{avg,fl} = \frac{T_{out} + T_{in}}{2} \tag{4}$$

The mesh dependency index is defined as eq. 5:

$$\theta = \left[\frac{|i_{grid,n} - i_{grid,n-1}|}{i_{grid,n}} \right] 100 \tag{5}$$

Where i is the variable studied. The mesh is considered sufficiently fine when θ is less than 2%. Table 4 lists results of the grid independence test for Re = 9 980 with the lattice structure in steel.

Table 4: Results of grid independence

Cell geometry	Elements	h_{eq} $(W.m^{-2}.K^{-1})$	θ (%)	ΔP (Pa)	θ (%)	Remark
BCCZ	728 496	14 427	2.2	15 787	8.5	
	2 398 169	14 748	1.3	14 550	0.1	
	5 335 699	14 945	-	14 579	-	Accepted
BCCZ+	762 605	13 608	15.1	24 684	14.0	
	1 917 637	16 036	1.4	21 660	0.4	
	4 334 934	16 265	-	21 580	-	Accepted
FCCZ	822 015	16 185	6.5	34 444	18.2	
	2 914 323	17 301	1.9	29 147	1.7	
	6 440 406	17 642	-	28 651	-	Accepted
FCCZ+	780 974	16 458	7.5	68 417	33.6	
	3 082 345	17 180	1.2	51 199	0.6	
	6 886 810	18 014	-	50 883	-	Accepted

5 Results and discussion

5.1 Model validation

Initially, numerical results are compared with experimental ones to validate the numerical model. To adapt the numerical domain to the experimental bench presented in section 3.1, it is necessary to consider the design of the heating element used experimentally and depicted in figure 5. Due to the low thermal conductivity of the polyimide film located between the heat flux applied with the steel sheet and the water circulation (the lower layer), there is a thermal gradient between its two surfaces. It is therefore necessary to take this polyimide film into account. Because of its very thin thickness, a very fine mesh is required for the film. Therefore, for fluid mechanics and heat transfer model validation, only a few lattice cells are considered, rather than the entire experimental test section. The upper layer of polyimide film is not taken into account because an adiabatic condition is assumed on its outer surface. The stainless steel sheet should be considered as it affects the thermal results. Numerical domain and boundary conditions for thermal validation are presented in figure 11.

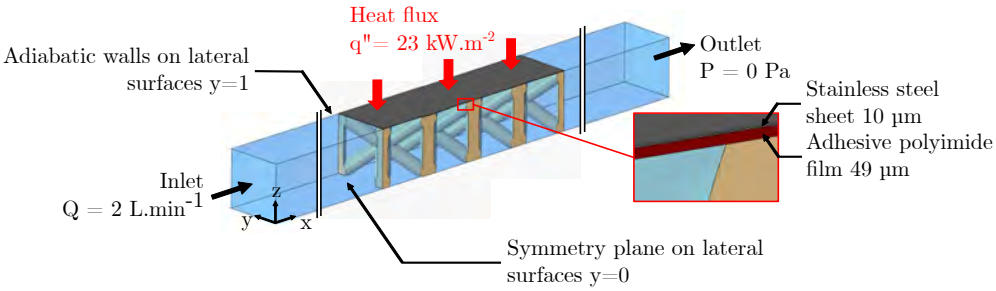

Fig. 11: Numerical domain and boundary conditions for thermal validation

The numerical and experimental temperature fields on two cells at steady state are shown in figure 12 and figure 13. Figure 13 shows the temperature along segment [AB], shown as a white dotted line in figure 12. This segment crosses a contact point between the heating element and the lattice structure.

Similar temperature fields are obtained both numerically and experimentally. The temperature distribution is not significantly homogenised by diffusion in the metallic heating plate due its thinness and moderate thermal conductivity. The maximum temperature difference on the dotted white line is $4°C$ between the numerical and experimental results. It can also be seen that the differences are localized at the contact between the lattice structure and the heating element. These slight temperature differences are perceptible between the numerical and experimental results due to bonding defects (glue point wider than the structure's ligament) between the structure and the heating element. Indeed, it has been experimentally observed that the adhesive point between the structure and the heating element affects the temperature field. The average temperature of the observed surface is denoted as $T_{avg,heater}$, and the value of the overall heat transfer coefficient is determined as eq 6:

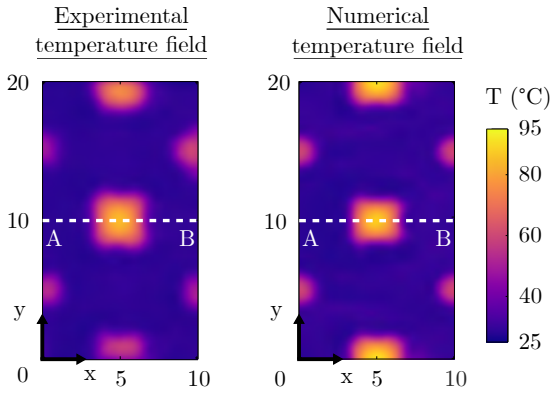

Fig. 12: Experimental and numerical temperature fields at the top of the heating element

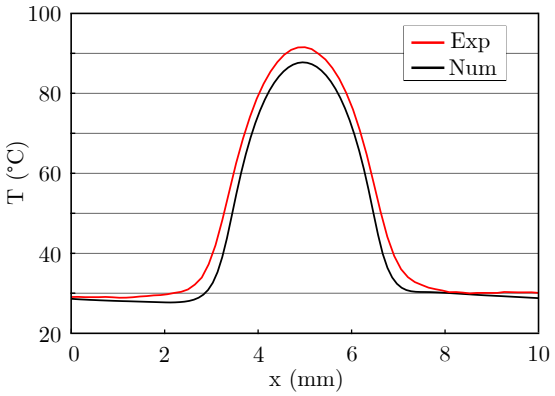

Fig. 13: Experimental and numerical temperatures along the segment [AB]

$$h_{eq,heater} = \frac{q"}{T_{avg,heater} - T_{in,fl}} \tag{6}$$

In table 5 difference of 6 % is observed on the value of the overall heat transfer coefficient between the experimental and numerical results, attributed to bonding defects between the lattice structure and the heating element. However, a good agreement is still noticeable between the numerical and experimental results.

For the validation of the fluid mechanics aspect, the experimental and numerical pressure drops at different flow rates are compared. The results are shown in figure 14. The graph shows the pressure drop results in the channel with the lattice structures used for several fluid flow rates. Both numerical and experimental pressure drop results are presented.

The maximum difference is about 4.3 % on the numerical and experimental pressure drop, which tends to validate the numerical simulation model.

Table 5: Comparison of numerical and experimental results

Variable	Simulation	Experiment
$T_{avg,heater}$ $(^{\circ}C)$	34.9	35.8
$h_{eq,heater}(W.m^{-2}.K^{-1})$	1 544	1 456
T_{min} $(^{\circ}C)$	27.7	27.1
T_{max} $(^{\circ}C)$	90.7	93.4

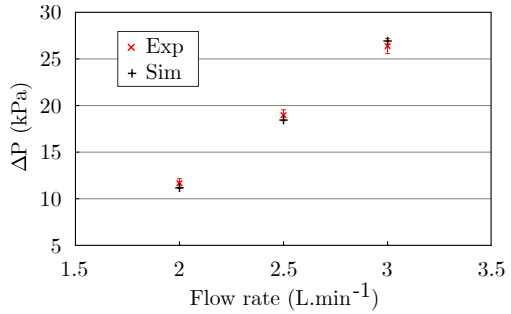

Fig. 14: Comparison of the simulation results with the measured data for pressure drop

5.2 Steady state

The system is first studied numerically in steady state, in order to carry out a local analysis of the physical phenomena, which would be difficult to achieve experimentally.

5.2.1 Global thermal-hydraulic performance and definition of the most efficient geometry

The first objective of the steady-state numerical analysis is to define which of the tested geometries presented in section 2 is the most efficient for use in tooling. To compare the thermo-hydraulic performance of different geometries it is necessary to introduce a performance index. For use in forming tools, both thermal and hydraulic performance are essential, so the performance index is chosen to take both aspects into account. The performance of the different configurations is estimated using a efficiency index defined as EI. For use in composites forming tools, in the case studied, three factors are important: heat transfer efficiency, pressure drop and temperature field homogeneity. The performance factor must therefore take these three elements into account. Heat transfer efficiency is considered by the Stanton number. Stanton number is a dimensionless quantity that expresses the relationship between the heat transfer coefficient and the heat capacity of a fluid defined as eq. 7:

$$St = \frac{h_{eq}}{\rho_{fl}\, v_{avg}\, cp_{fl}} \tag{7}$$

Where ρ_{fl} is the density of the fluid, v_{avg} the mean velocity of the fluid and cp_{fl} the specific heat capacity of the fluid.

Pressure drop is taken into account by the dimensionless factor f :

$$f = \frac{2\,\Delta P\,D_h}{L\,\rho_{fl}\,v_{avg}^2} \tag{8}$$

Where L is the channel length. The hydraulic diameter D_h of the lattice channel is defined as eq. 9 [40]:

$$D_h = \frac{4\,V_{fl}}{A_w} \tag{9}$$

Where V_{fl} is the fluid volume and A_w the wetted surface area.

Finally, the homogeneity of the temperature field is taken into account with the standard deviation $\sigma_{T_{ts}}$ of the temperature on the tooling surface. A low standard deviation reflects a uniform temperature field at the contact surface with the composite part.

The performance index EI is then defined as :

$$EI = \frac{\frac{St}{St_0}}{(\frac{f}{f_0})^{\frac{1}{3}}}\,\frac{\sigma_{T_0}}{\sigma_{T_{ts}}} \tag{10}$$

Where St_0, f_0 and σ_{T_0} are respectively the Stanton number, the friction factor and the standard deviation of temperature at the tooling surface for the empty channel. This performance index is used to select the geometry which provides the best ratio of thermal and hydraulic performance.

To analyze the global thermal performance of tested geometries, figure 15 presents the temperature evolution along a line in the fluid flow direction at the tooling surface : $T(x)$ on the segment [AB]. Simultaneously, the figure illustrates the heat temperature evolution $T(x)$ along a line in the fluid flow direction at the fluid-solid interface on the segment [CD]. Figure 15 a) and b) show temperature evolution along the whole length, and c) and d) only along the sixth cell. Segment [CD] is chosen to avoid crossing of the ligaments of the lattice structure for each geometry, and segment [AB] is positioned above [CD] on the tooling surface. All lattice structure geometries presented in section 2 are tested in stainless steel and polymer. Polymer material is less thermally conductive but has the advantage to be easier to manufacture in AM. Its use can be envisaged for forming processes where the pressure on the surface of the tool is low enough.

In all cases, the temperature is lower for configurations with lattice structures than for the empty channel, demonstrating the improved heat transfer achieved by using these structures. The temperature evolution at the tooling surface is lower along the fluid flow than for the empty channel, whatever the lattice structure. This shows that lattice structures improve the uniformity of the temperature field. Temperature variations at the fluid-solid interface and at the tool surface are similar for each geometry, but for the same structure, depending on the material, the temperature varies by around 2 $^{\circ}C$. For temperature at the fluid-solid interface, periodic variations are visible. These temperature peaks where the local temperature varies at the fluid-solid

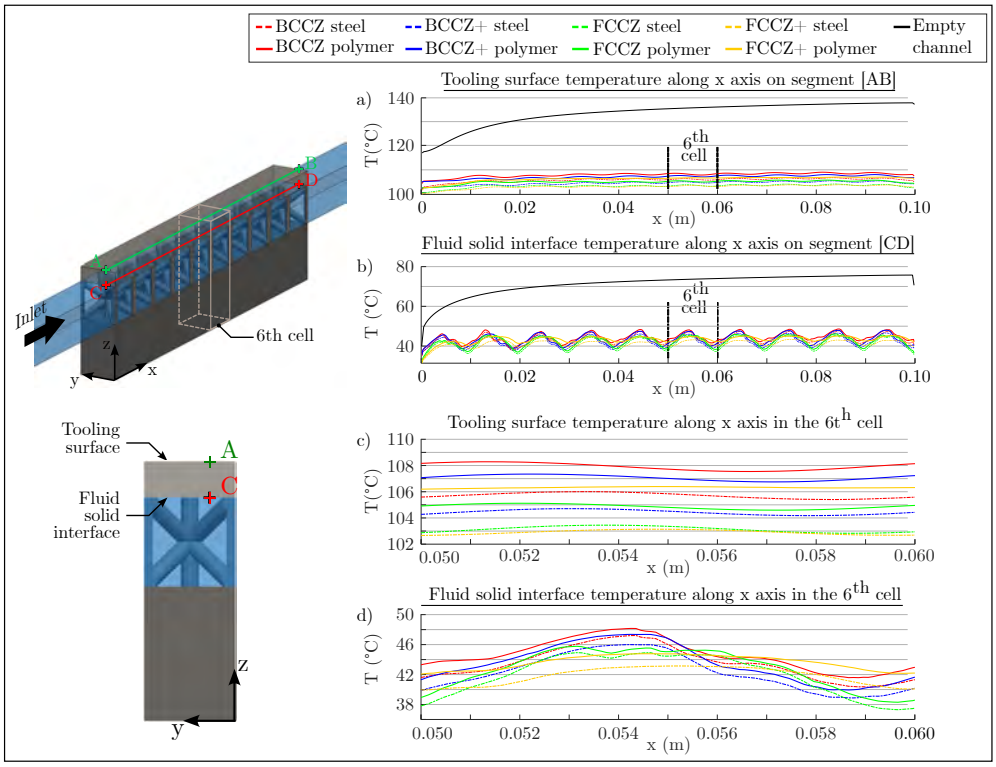

Fig. 15: Temperature evolution along x axis on tooling surface and fluid solid interface

interface with the lattice structure correspond to zones where the passage cross-section is reduced, and therefore where fluid velocity and turbulence are increased. These local variations lead to a minimum thickness of the upper part to ensure a homogeneous temperature at the tooling surface, which is essential for the production of composite parts.

Table 6 presents the numerical average temperature of the tooling surface on the segment [AB] $T_{avg,line,ts}$ (figure 15), the global heat transfer coefficient h_{eq} and the pressure drop for the different geometries and materials.

The tooling surface temperature decreases considerably with the lattice structure compare to the empty channel for the same inlet velocity. The global heat transfer coefficient h_{eq} is approximately three times higher than empty channel for all geometries. The geometry strongly impacts the pressure drop of the systems.

Figure 15 and table 6 shows that face-centered cubic structures appear to be the best in terms of heat transfer. However, the hydraulic performance aspect also needs to be taken into account as mentioned previously. Table 7 presents results of efficiency index previously defined of the different geometries and structure's material.

Table 7 shows that the Stanton number is similar for all geometries. Concerning the influence of the conductivity of the lattice structure, although the stainless steel lattice structure has a thermal conductivity more than 70 times higher than the polymer one,

Table 6: Numerical results of the different geometries

Cell geometry	Lattice structure material	$T_{avg,line,ts}$ $(^{\circ}C)$	h_{eq} $(W.m^{-2}.K^{-1})$	ΔP (kPa)
BCCZ	Stainless steel	105.7	14 945	14.58
	Polymer	107.5	13 285	
BCCZ+	Stainless steel	103.9	16 265	21.58
	Polymer	106.5	14 018	
FCCZ	Stainless steel	102.7	17 642	28.50
	Polymer	104.5	15 802	
FCCZ+	Stainless steel	102.4	18 014	50.88
	Polymer	105.7	14 966	
Empty channel	-	133.3	5 573	0.70

Table 7: Efficiency index of the different geometries and structure's material

Cell geometry	Lattice structure material	St	$\frac{St}{St_0}$	f	$\frac{f}{f_0}$	$\sigma_{T_{ts}}$ $(^{\circ}C)$	EI
BCCZ	Stainless steel	$2.98.10^{-3}$	2.34	0.93	17.81	1.0	4.3
	Polymer	$2.65.10^{-3}$	2.08			1.0	3.8
BCCZ+	Stainless steel	$3.25.10^{-3}$	2.84	1.38	26.37	0.8	5.1
	Polymer	$2.80.10^{-3}$	2.19			0.8	4.4
FCCZ	Stainless steel	$3.52.10^{-3}$	2.76	2.22	42.39	0.8	4.8
	Polymer	$3.16.10^{-3}$	2.47			0.8	4.3
FCCZ+	Stainless steel	$3.60.10^{-3}$	2.82	3.80	72.71	1.0	3.2
	Polymer	$2.99.10^{-3}$	2,24			1.1	2.5
Empty channel		$1.27.10^{-3}$	1	0.05	1	4.8	1

the Stanton number is only increased between 11 % and 15%. This result shows that in this configuration, for the same geometry and flow condition, the material of the lattice structure has a little impact on thermal exchanges. This result is in agreement with the work of Fuller & al [35]. The FCCZ+ geometry is considered the less efficient for the intended application, due to its high pressure drop because of smaller passage sections, which impede the passage of fluid for similar thermal performance. This result in a lower efficiency index. The BCCZ+ geometry is considered the most efficient in terms of the ratio between thermal and hydraulic performance, this is why BCCZ+ geometry is retained in the rest of this study.

As the BCCZ+ structure is considered the most efficient efficient for composite tooling applications, whatever the material used, the rest of the study will focus on it.

5.2.2 Heat transfer analysis for BCCZ+ structure

With the geometry considered to be the most efficient identified, a local analysis of the coupling between fluid flow and heat transfer is carried out. The aim of this section is to analyze the heat transfer distribution in configuration studied.

In the studied system, the first type of dissipation is convection between the fluid and the upper part (on the blue surface in figure 16), which will be referred to as

direct convection. The second type of dissipation is convection between the fluid and the heat conducted through the ligaments of the structure (that can be considered as fin) referred to as indirect convection. To analyze fin efficiency, heat flux evacuated through the ligament (indirect convection) is compared to the flux evacuated on the direct contact between the fluid and the upper plate (direct convection). The interface between the lattice structure and the upper part is represented in red in figure 16 and designated as $A_{cl,up}$, while the interface between the fluid and the upper part is illustrated in blue and referred to as $A_{cf,up}$.

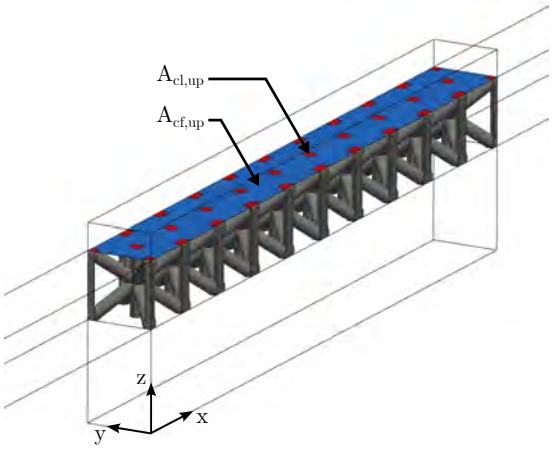

Fig. 16: Scheme of the different surfaces in contact with the upper part

The proportion of contact surface between the lattice structure and the upper part $\Gamma_{cl,up}$ is given by eq. 11:

$$\Gamma_{cl,up} = \frac{A_{cl,up}}{A_{tot}} \tag{11}$$

Where A_{tot} is the total area of the upper part :

$$A_{tot} = A_{cl,up} + A_{cf,up} \tag{12}$$

The heat flux evacuated by direct convection between the fluid and the upper plate is noted $\phi_{cf,up}$ and the one evacuated by indirect convection $\phi_{cl,up}$. The proportion of heat flux dissipated in the lattice structure is defined by eq. 13:

$$\eta_{cl,up,simulation} = \frac{\phi_{cl,up}}{\phi_{tot}} \tag{13}$$

Where $\phi_{tot} = \phi_{cl,up} + \phi_{cf,up}$. Table 8 presents the proportion of heat flux evacuated by conduction in the ligaments from the simulation in function of the lattice structure material. The ratio between heat flux transferred by the ligaments of the lattice structure $\eta_{cl,up,simulation}$ and the surface area occupied by the contact between the lattice structure and the upper plate $\Gamma_{cl,up}$ is also shown.

Table 8: Proportion of heat flux evacuated in the ligament of the structure

Lattice structure material	$\Gamma_{cl,up}$ (%)	$\eta_{cl,up,simulation}$ (%)	$\eta_{cl,up,simulation}/\Gamma_{cl,up}$
Polymer	9.1	0.5	0.055
Stainless steel	9.1	9.8	1.077

The table 8 shows that the heat flux dissipated by conduction in the ligaments is impacted by the thermal conductivity of the lattice structure, for the same value of $\Gamma_{cl,up}$, the value of $\eta_{cl,up}$ is divided by around 20 in the case of the polymer.

The value of the ratio $\eta_{cl,up,simulation}/\Gamma_{cl,up}$ shows that in this configuration, the fin effect associated with the lattice structure is not the driving force behind improved heat transfer, with a value just over 1 in the case of the steel lattice structure. These results show that it is not the increase in exchange surface area induced by the lattice structure that improves heat transfer in this configuration. In fact, for the stainless steel lattice structure, over 90% of the heat flux is dissipated by direct convection, and almost the entire heat flux for the polymer lattice structure. Fluid flow, which has a direct impact on this direct convection between the fluid and the upper part is analyzed in the following section.

In this configuration, evacuation of the heat flux takes place mainly by direct convection between the fluid and the upper plate. These results explain the small difference of h_{eq} in table 6 between a polymer lattice structure and a stainless steel one. The impact of the structure's material also has little impact on the h_{eq} coefficient, as contact surface $\Gamma_{cl,up}$ represents only 9.1 % of the total exchange surface.

5.2.3 Fluid flow analysis inside BCCZ+ structure

Direct convection is the dominant mode of heat transfer in the cases considered in this work. The nature and properties of fluid flow are therefore studied in this section. Figure 17 shows streamlines and normalized velocity magnitude on two orthogonal planes defined in a single cell, the sixth, not located in the region affected by the entry into or exit from the lattice structure. The plane P1 (on the XY plane) is localized just under the upper part, at 0.25 mm to avoid having a zero velocity field corresponding to the no-slip condition. The plane P2 (on the XZ plane) is located at 2.5mm of the cell extremity. The reduced passage generated by the lattice structures causes local acceleration of the fluid, with a speed of up to three times the entry speed. This phenomenon obviously favours convective transfers. As well as increasing velocity, the ligaments generate vortex zones. In fact, in the vicinity of the ligaments, significant recirculations of the flow are observed and the lattice structure induces strong tortuosity, increasing heat transfer.

Figure 18 illustrates the turbulence kinetic energy (TKE) distribution on the plane P1, and the temperature distribution of the lower face of the upper part: plane P3, located at the interface between the upper part the fluid and the lattice structure. The TKE is determined by measuring root-mean-square velocity fluctuations, which offer valuable insights into the intensity of turbulence flow mixing. Elevated TKE levels contribute to enhanced flow mixing, resulting in enhanced heat transfer capabilities.

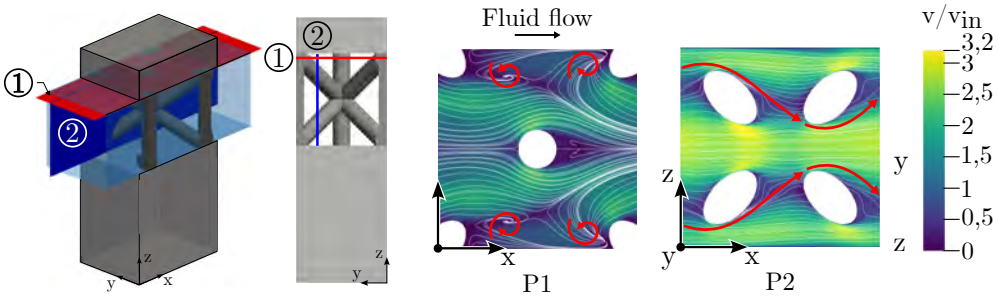

Fig. 17: Streamlines superimposed with normalized velocity contours on two planes

Figure 18 shows that the temperature distribution is directly related to the turbulence kinetic energy, zones with higher TKE present lower temperatures (white dotted area). The ligaments that increase this turbulent energy on plane P1 and heat transfer are those inclined at 45 degrees to the z axis, rather than the one parallel to the z axis in the center of the cell. Indeed, they reduce the cross-sectional area between the fluid and the exchange surface, and direct part of the fluid flow towards the top plate. The lattice structure acts as a turbulence amplifier which contributes the improve thermal transfer. From the temperature fields shown in figure 18 (plane P3), it can be seen that the contact zones between the lattice structure and the upper part have a higher temperature for the polymer structure due to its lower thermal conductivity.

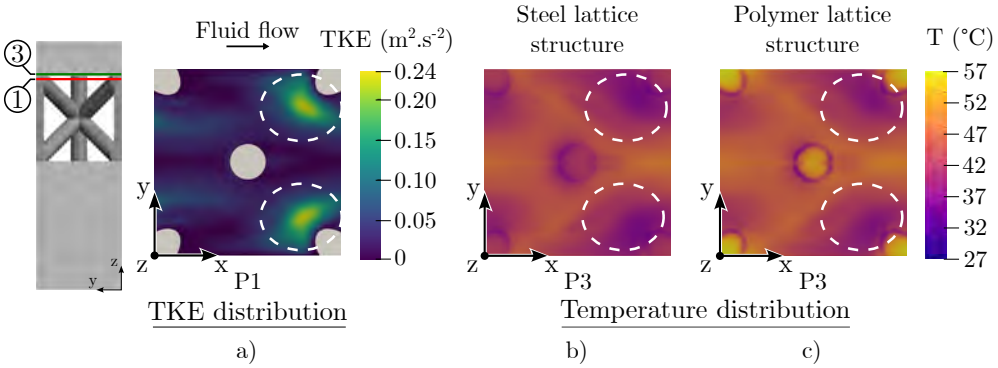

Fig. 18: a) Turbulence kinetic energy TKE of the fluid on plane 1 (red line on the diagram) and temperature distribution on plane 3 (green line on the diagram) for the configuration with b) stainless steel lattice structure and c) polymer lattice structure

Figure 19 displays the fluid temperature field on the plane P2. As shown in figure 17, the lattice structure provides an acceleration of fluid flow and vortices near to the exchange surface. These characteristics allow to disrupt the thermal boundary layer formed by the heat flux applied. Disruption of this thermal boundary layer improves heat exchange and homogeneity of temperature distribution on the tooling surface.

Accordingly, disturbance of this thermal boundary layer with the lattice structure limits the temperature gradient in the direction of fluid flow (x axis) in comparison to an empty channel where the size and temperature of the thermal boundary layer increases in the fluid flow direction. It explains the better temperature field homogeneity by using lattice structures.

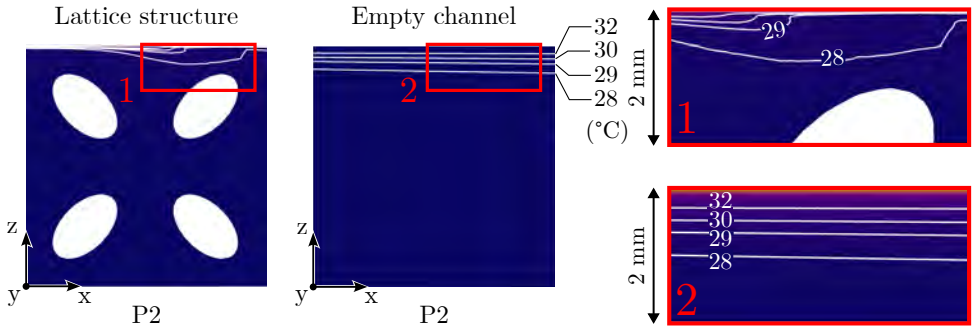

Fig. 19: Fluid temperature isotherms on plane 2 for an empty channel and a channel with BCCZ+ lattice structure. Isotherms at 28 $^{\circ}C$, 29 $^{\circ}C$, 30 $^{\circ}C$, 32 $^{\circ}C$

This numerical work shows that the improvement in heat transfer is linked both to the increase in fluid velocity and to the vortices generated by the lattice structure. Lattice structure generates significant fluid mixing and high TKE, which improve convective exchanges.

5.3 Transient state

The transient state is studied experimentally, due to the numerical cost generated by transient simulations. The aim of this unsteady-state section is to study the system in a cyclic regime consisting of heating and cooling phases. In response to these cycles, the uniformity of the temperature field at the tooling surface, as well as the heating and cooling rates, are studied. In this transient analysis, two channel configurations are used. The first configuration is a channel with a BCCZ+ lattice structure of constant porosity to ensure a uniform temperature at the tooling surface during heating and cooling phases. Then, a second configuration is used, with a non-constant porosity of the BCCZ+ lattice structure in the channel, to obtain a local variation of the temperature which can be useful for example in cases of composite parts with thickness variation.

5.3.1 Configuration 1: constant porosity

Figure 20 shows the temporal evolution of the water temperature at the entrance to the test section in green line, the mean temperature (solid line) and the standard deviation *Std* (dotted line) of the temperature on the upper surface of the stainless steel plate: the tooling surface. Firstly, it can be seen that that when the fluid temperature

changes, the temperature does not instantly match the setpoint. This is due to the small volume of thermoregulators, which means that the temperature is influenced by the fluid returning inside, being either hotter or colder than the set point. Then, the difference between the hot stationary temperatures at the tooling surface is linked to the ratio between the heat transfer coefficient with the ambient air at the tooling surface and the one between the fluid and the tooling skin, which is smaller when the lattice structure is present. The heating and cooling rates of the tooling surface are increased thanks to the structure. Note that the standard deviation is reduced during transient phases when lattice structures are added. This means that the temperature at the tooling surface is more uniform.

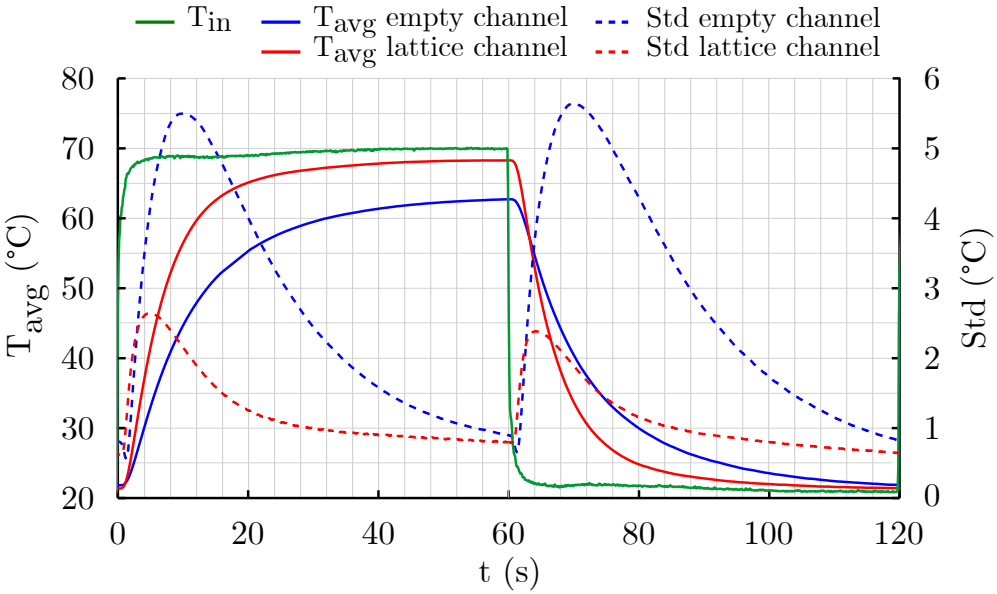

Fig. 20: Temporal evolution of the mean and standard deviation of the temperature on the observed surface

Thermal inertia of the tooling skin is characterized by the thermal time constant τ, the time to reach 63.2 % of the temperature amplitude, in this case 51 $^{\circ}C$ with the lattice channel and 48.5 $^{\circ}C$ for the empty channel. The steady state is reached at the value of 5τ. Results are presented in table 9. The time to obtain the steady state is reduced by 38 % in this configuration thanks to the lattice structure.

Table 9 presents also heating and cooling rates for the empty channel and the lattice one for the period from 0 s to the thermal time constant τ. The lattice structure allows to increase the heating and cooling rates by about 77% compare to the empty channel.

Figure 21 presents thermographies (31x313 pixels resolution) of the tooling surface at the same time $t = 10\ s$ after the beginning of the cooling (corresponding to 70 s in figure 20) for the empty channel and for the lattice one. Figure 22 presents the

Table 9: Thermal time constant, heating and cooling rates for both configurations for both configurations

	τ (s)	5τ (s)	Heating / Cooling rates $\Delta T/\Delta t$ $(^{\circ}C.s^{-1})$
Lattice structure	7.7	38.5	3.9
Empty channel	12.5	62.5	2.2

temperature evolution at the tooling surface along the fluid flow on the segment [AB] at several time of cooling 5, 10, 15 and 20 seconds, corresponding to 65, 70, 75 and 80 seconds in figure 22.

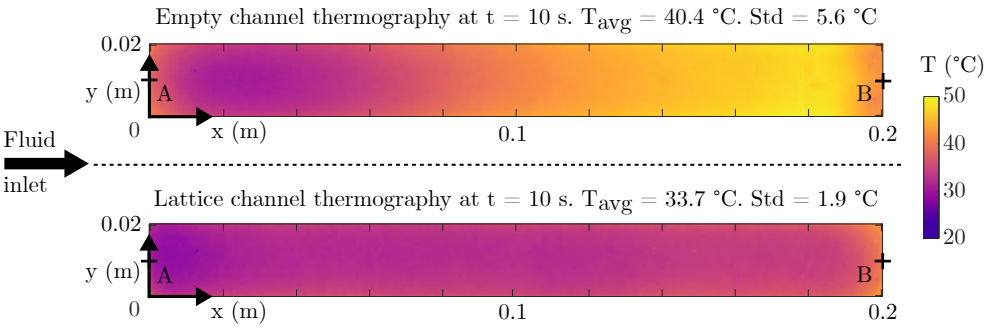

Fig. 21: Empty channel and lattice channel thermal imaging at 10 seconds of cooling

Figures 21 and 22 highlight the improved uniformity of the temperature field at the tooling surface, thanks to the lattice structure, during the entire transient phase. This improvement in temperature field uniformity in the flow direction can be linked to the disturbance of the thermal boundary layer obtained with the lattice structure, as presented in the numerical section.

Table 10 presents the maximum temperature difference on segment [AB] at the tooling surface during the cooling phase. The difference is measured between $x = 0.02$ m and $x = 0.18$ m, in order to not consider the effects of the inlet and outlet zones.

Table 10: Maximum temperature difference at the tooling surface on segment [AB] during the cooling phase

t (s)	5	10	15	20
Lattice structure ΔT_{max} $(^{\circ}C)$	5.2	3.5	2.1	1.1
Empty channel ΔT_{max} $(^{\circ}C)$	13.5	16.9	15.0	12.4

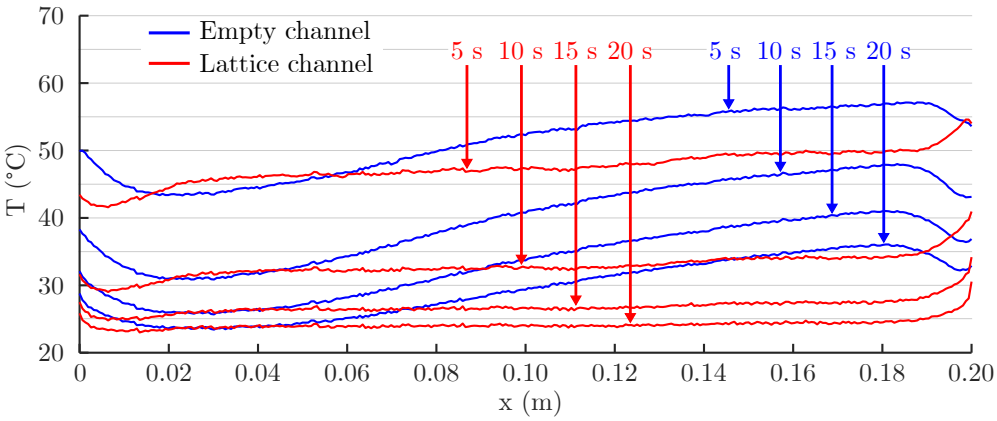

Fig. 22: Temperature evolution at the tooling surface during cooling phase along x axis on the segment [AB] at different cooling times

Table 10 shows that the temperature gradient along the fluid flow is reduced up to 11 times by using the lattice structure, although higher heating and cooling rates. This ensure more uniform cooling of the produced part.

5.3.2 Configuration 2: non-constant porosity

Using lattice structures enables to locally modified its porosity ε in order to control heat transfer and therefore the tooling surface temperature. Yun & al [32] have shown that by decreasing porosity for a constant imposed flow rate, heat transfers are increased. As the porosity decreases, vortices inside the lattice channel become more prominent, and near-wall flow velocities are intensified, causing larger disturbance of the thermal boundary layer as seen previously. These two phenomena improve convective heat transfers. The configuration adopted here is a cells porosity of $\varepsilon = 0.8$ at the beginning of the channel (10 cells), then, $\varepsilon = 0.5$ (4 cells) and finally $\varepsilon = 0.8$ (6 cells). The objective is, with a single fluid inlet temperature, to locally control the temperature field on the surface of the tool. Figure 23 presents the lattice structures integrated into the channel and thermal imaging of the tooling surface at 5 seconds of cooling (t = 65 s in figure 20). Figure 24 presents temperature evolution at the tooling surface at 5 seconds of cooling along x axis on the segment [AB] for graded porosity channel.

Between $x = 0\ m$ and $x = 0.02\ m$, the area is affected by the inlet which explains the lower temperature. Then, the temperature is immediately reduced at the start of the porosity change at $x = 0.1\ m$, but when the porosity returns to $\epsilon = 0.8$ at $x = 0.14\ m$, the temperature change is not immediate, as the fluid flow does not regain its initial velocity as soon as the porosity increases. In this configuration temperature can be locally decrease of $5°C$ at the tooling surface after 5 seconds of cooling compared to the rest of the channel. This means that it is possible to locally control the temperature distribution at the tooling surface with a unique inlet temperature of the fluid by adapting lattice structure porosity in space. The future objective is to adapt the temperature field of the tooling surface to the part to be manufactured.

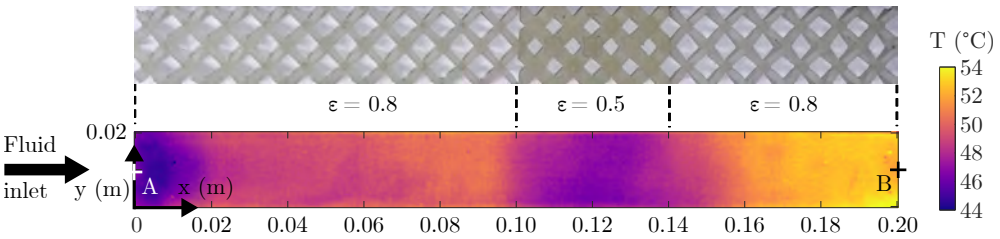

Fig. 23: Thermal imaging of the tooling surface after 5 seconds of cooling for the graded porosity channel

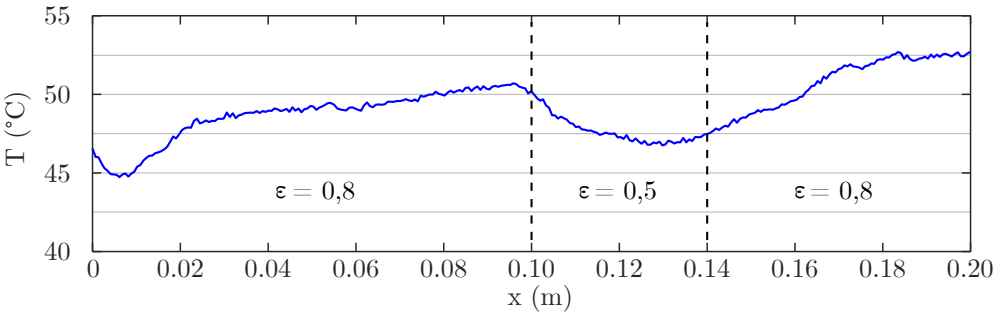

Fig. 24: Temperature evolution at the tooling surface after 5 seconds of cooling along x axis on the segment[AB] for graded porosity channel

6 Conclusion

The use of lattice structures for thermal management of forming tools for the manufacture of composite parts, for example by thermo-stamping or injection molding, improves the thermal efficiency of the tooling.

In this study, global thermo-hydraulic performances of different geometries of lattice structures are compared. Numerical results show that geometry of the structure has a stronger influence on the pressure drop than on the heat transfers. The material of the lattice structure has a little impact on the thermal performance of the system in the studied configuration, with water and high Reynolds number. Using an efficiency index based on the ratio between thermal and hydraulic performance, it has been demonstrated that the BCCZ+ geometry offers the best performance index. It is shown that the porous structure acts rather as a turbulence amplifier, and the fin effect is not the predominant phenomenon in terms of heat transfer in the studied configuration. Convective heat transfers are enhanced by increased fluid velocity, vortex zones and disturbance of the thermal boundary layer. For that reason, conductivity of the lattice structure doesn't affect significantly heat transfer, which makes it possible to use a less expensive polymer structure, if it satisfies the criterion of mechanical resistance expected for the forming process.

Experimentally, it is shown that the lattice structure makes it possible to obtain rapid temperature variations with good temperature uniformity during the thermal

transient phases. The time constant is reduced by using the lattice structure. It is also possible to concentrate heat transfers by adapting porosity of the structure to manufacture composite parts with thickness variation. The use of lattice structures for the thermal management of tooling would then make it possible to increase the quality of the parts produced by finely controlling the temperature field at the surface of the tooling, while reducing the time of heating or cooling of shaped parts. However, certain technological issues are not addressed in this work, such as the presence of residues in the fluid (due to wear of the lattice structures, or other tooling components) which could compromise the system by clogging pores or wearing ligaments of the lattice structures.

Compared to the conformal cooling, thermal inertia can be greatly improved thanks to the lattice structure which allows the circulation of the fluid as close as possible to the surface of the tool without thermal marking. By circulating the fluid as close as possible to the tooling surface, the mass to heat and cool is reduced, resulting in lower energy consumption. Indeed, in real case, channels of conformal cooling are located at one time the diameter of the channel which is not the case in this paper.

Although this study does not take into account the composite part, but only the tooling, ensuring a controlled temperature field on the surface of the tooling guarantees the right temperature inside the part. This study is based on a fluid which is water, but in some cases it is necessary to use high temperatures, which requires the use of another heat transfer fluid, oil for example. The results could then be different, with thermal conductivity of the lattice structure having a greater impact on heat exchange. The flow rate of the fluid, and therefore the Reynolds number also impact these results.

References

[1] Bushko, W. C. & Stokes, V. K. Solidification of thermoviscoelastic melts. part 3: Effects of mold surface temperature differences on warpage and residual stresses. *Polymer Engineering & Science* **36**, 322–335 (1996). URL https://4spepublications.onlinelibrary.wiley.com/doi/10.1002/pen.10419.

[2] Sánchez, R., Aisa, J., Martinez, A. & Mercado, D. On the relationship between cooling setup and warpage in injection molding. *Measurement* **45**, 1051–1056 (2012). URL https://linkinghub.elsevier.com/retrieve/pii/S0263224112000541.

[3] Agazzi, A., Sobotka, V., LeGoff, R. & Jarny, Y. Inverse method for the cooling system design in injection moulding – application to a 't-shaped' piece **22**, 707–726 (2014). URL https://www.tandfonline.com/doi/full/10.1080/17415977.2013.823412.

[4] McCool, R. *et al.* Thermoforming carbon fibre-reinforced thermoplastic composites. *Proceedings of the Institution of Mechanical Engineers, Part L: Journal of Materials: Design and Applications* **226**, 91–102 (2012). URL http://journals.sagepub.com/doi/10.1177/1464420712437318.

[5] Bahnini, I., Rivette, M., Rechia, A., Siadat, A. & Elmesbahi, A. Additive manufacturing technology: the status, applications, and prospects. *The International Journal of Advanced Manufacturing Technology* **97** (2018). URL http://link.springer.com/10.1007/s00170-018-1932-y.

[6] Li, N. *et al.* Progress in additive manufacturing on new materials: A review. *Journal of Materials Science & Technology* **35**, 242–269 (2019). URL https://linkinghub.elsevier.com/retrieve/pii/S1005030218301786.

[7] Niknam, S. A., Mortazavi, M. & Li, D. Additively manufactured heat exchangers: a review on opportunities and challenges. *The International Journal of Advanced Manufacturing Technology* **112**, 601–618 (2021). URL http://link.springer.com/10.1007/s00170-020-06372-w.

[8] Saifullah, A. B. M. & Masood, S. H. Finite element thermal analysis of conformal cooling channels in injection moulding. *5 th Australasian Congress on Applied Mechanics, ACAM* (2007).

[9] Wang, Y., Yu, K.-M., Wang, C. C. & Zhang, Y. Automatic design of conformal cooling circuits for rapid tooling. *Computer-Aided Design* **43**, 1001–1010 (2011). URL https://linkinghub.elsevier.com/retrieve/pii/S0010448511001060.

[10] Berger, G. R., Zorn, D., Friesenbichler, W., Bevc, F. & Bodor, C. J. Efficient cooling of hot spots in injection molding. a biomimetic cooling channel versus a heat-conductive mold material and a heat conductive plastics. *Polymer Engineering & Science* **59** (2019). URL https://4spepublications.onlinelibrary.wiley.com/doi/10.1002/pen.25024.

[11] Jahan, S., Wu, T., Shin, Y., Tovar, A. & El-Mounayri, H. Thermo-fluid topology optimization and experimental study of conformal cooling channels for 3d printed plastic injection molds. *Procedia Manufacturing* **34**, 631–639 (2019). URL https://linkinghub.elsevier.com/retrieve/pii/S2351978919308480.

[12] Heogh, W. *et al.* The design and additive manufacturing of an eco-friendly mold utilized for high productivity based on conformal cooling optimization. *Materials & Design* **222**, 111088 (2022). URL https://linkinghub.elsevier.com/retrieve/pii/S0264127522007109.

[13] Agazzi, A., Sobotka, V., Le Goff, R., Garcia, D. & Jarny, Y. A methodology for the design of effective cooling system in injection moulding. *International Journal of Material Forming* **3**, 13–16 (2010). URL http://link.springer.com/10.1007/s12289-010-0695-2.

[14] Hopmann, C. & Nikoleizig, P. Inverse thermal mold design for injection molds: Adressing the local cooling demand as quality function for an inverse heat transfer problem. *International Journal of Material Forming* **11**, 113–124 (2018). URL http://link.springer.com/10.1007/s12289-016-1334-3.

[15] Hopmann, C., Gerads, J. & Hohlweck, T. Investigation of an inverse thermal injection mould design methodology in dependence of the part geometry. *International Journal of Material Forming* **14**, 309–321 (2021). URL http://link.springer.com/10.1007/s12289-020-01604-6.

[16] Reyes, E., Tardif, X., Bailleul, J.-L., Allanic, N. & Sobotka, V. Inverse heat transfer optimization of stamping with over-molding process involving high performance thermoplastic composites: experimental validation. *International Journal of Material Forming* **15**, 5 (2022). URL https://doi.org/10.1007/s12289-022-01648-w.

[17] Kanbur, B. B., Suping, S. & Duan, F. Design and optimization of conformal cooling channels for injection molding: a review. *The International Journal of Advanced Manufacturing Technology* **106**, 3253–3271 (2020). URL http://link.springer.com/10.1007/s00170-019-04697-9.

[18] Arman, S. & Lazoglu, I. A comprehensive review of injection mold cooling by using conformal cooling channels and thermally enhanced molds. *The International Journal of Advanced Manufacturing Technology* **127**, 2035–2106 (2023). URL https://link.springer.com/10.1007/s00170-023-11593-w.

[19] Mercado-Colmenero, J. M., Martin-Doñate, C., Rodriguez-Santiago, M., Moral-Pulido, F. & Rubio-Paramio, M. A. A new conformal cooling lattice design procedure for injection molding applications based on expert algorithms. *The International Journal of Advanced Manufacturing Technology* **102**, 1719–1746 (2019). URL http://link.springer.com/10.1007/s00170-018-03235-3.

[20] Kuo, C.-C., Jiang, Z.-F., Yang, X.-Y., Chu, S.-X. & Wu, J.-Q. Characterization of a direct metal printed injection mold with different conformal cooling channels. *The International Journal of Advanced Manufacturing Technology* **107**, 1223–1238 (2020). URL http://link.springer.com/10.1007/s00170-020-05114-2.

[21] Wilson, N. *et al.* Analysis of self-supporting conformal cooling channels additively manufactured by hybrid directed energy deposition for IM tooling. *The International Journal of Advanced Manufacturing Technology* (2024). URL https://doi.org/10.1007/s00170-024-13291-7.

[22] Au, K. & Yu, K. Modeling of multi-connected porous passageway for mould cooling. *Computer-Aided Design* **43**, 989–1000 (2011). URL https://linkinghub.elsevier.com/retrieve/pii/S0010448511000418.

[23] Ngo, T. D., Kashani, A., Imbalzano, G., Nguyen, K. T. & Hui, D. Additive manufacturing (3d printing): A review of materials, methods, applications and challenges. *Composites Part B: Engineering* **143**, 172–196 (2018). URL https://linkinghub.elsevier.com/retrieve/pii/S1359836817342944.

[24] Hussein, A., Hao, L., Yan, C., Everson, R. & Young, P. Advanced lattice support structures for metal additive manufacturing. *Journal of Materials Processing Technology* **213**, 1019–1026 (2013). URL https://linkinghub.elsevier.com/retrieve/pii/S092401361300037X.

[25] Riva, L., Ginestra, P. S. & Ceretti, E. Mechanical characterization and properties of laser-based powder bed–fused lattice structures: a review. *The International Journal of Advanced Manufacturing Technology* **113**, 649–671 (2021). URL http://link.springer.com/10.1007/s00170-021-06631-4.

[26] Maconachie, T. *et al.* Slm lattice structures: Properties, performance, applications and challenges. *Materials and Design* **183** (2019).

[27] Yánez, A., Fiorucci, M. P., Cuadrado, A., Martel, O. & Monopoli, D. Surface roughness effects on the fatigue behaviour of gyroid cellular structures obtained by additive manufacturing **138**, 105702 (2020). URL https://linkinghub.elsevier.com/retrieve/pii/S0142112320302334.

[28] Brooks, H. & Brigden, K. Design of conformal cooling layers with self-supporting lattices for additively manufactured tooling. *Additive Manufacturing* **11**, 16–22 (2016). URL https://linkinghub.elsevier.com/retrieve/pii/S2214860416300409.

[29] Lepoivre, A. *et al.* Rapid heat control for thermoplastic injection tooling using lattice structures as heat exchanger. *Key Engineering Materials* **926**, 1850–1863 (2022). URL https://www.scientific.net/KEM.926.1850.

[30] Valentine, M. D. A. *et al.* Additively manufactured cure tools for composites manufacture. *The International Journal of Advanced Manufacturing Technology* **127**, 4237–4251 (2023). URL https://link.springer.com/10.1007/s00170-023-11254-y.

[31] Alessio, F., Alessio, M., Savoldelli, P., Vedani, M. & Viganò, R. Design of additively manufactured moulds for expanded polymers. *The International Journal of Advanced Manufacturing Technology* **125**, 4899–4908 (2023). URL https://link.springer.com/10.1007/s00170-023-10936-x.

[32] Yun, S., Kwon, J., Lee, D., Shin, H. H. & Kim, Y. Heat transfer and stress characteristics of additive manufactured FCCZ lattice channel using thermal fluid-structure interaction model. *International Journal of Heat and Mass Transfer* **149**, 119187 (2020). URL https://linkinghub.elsevier.com/retrieve/pii/S0017931019351671.

[33] Dixit, T., Nithiarasu, P. & Kumar, S. Numerical evaluation of additively manufactured lattice architectures for heat sink applications. *International Journal of Thermal Sciences* **159**, 106607 (2021). URL https://linkinghub.elsevier.com/retrieve/pii/S1290072920310577.

[34] Liang, D., Bai, W., Chen, W. & Chyu, M. K. Investigating the effect of element shape of the face-centered cubic lattice structure on the flow and endwall heat transfer characteristics in a rectangular channel. *International Journal of Heat and Mass Transfer* **153**, 119579 (2020). URL https://linkinghub.elsevier.com/retrieve/pii/S0017931019345685.

[35] Fuller, A. J., Kim, T., Hodson, H. P. & Lu, T. J. Measurement and interpretation of the heat transfer coefficients of metal foams. *Proceedings of the Institution of Mechanical Engineers, Part C: Journal of Mechanical Engineering Science* **219**, 183–191 (2005). URL http://journals.sagepub.com/doi/10.1243/095440605X8414.

[36] Leary, M. *et al.* Inconel 625 lattice structures manufactured by selective laser melting (slm): Mechanical properties, deformation and failure modes. *Materials and Design* **157**, 179–199 (2018). URL https://www.sciencedirect.com/science/article/pii/S0264127518304763.

[37] Naqiuddin, N. H. *et al.* Numerical investigation for optimizing segmented microchannel heat sink by taguchi-grey method. *Applied Energy* **222**, 437–450 (2018). URL https://linkinghub.elsevier.com/retrieve/pii/S0306261918305336.

[38] Yun, S., Lee, D., Jang, D. S., Lee, M. & Kim, Y. Numerical analysis on thermo-fluid–structural performance of graded lattice channels produced by metal additive manufacturing. *Applied Thermal Engineering* **193**, 117024 (2021). URL https://linkinghub.elsevier.com/retrieve/pii/S1359431121004701.

[39] Celik, I. B. *et al.* Procedure for estimation and reporting of uncertainty due to discretization in CFD applications. *Journal of Fluids Engineering* **130**, 078001 (2008). URL http://FluidsEngineering.asmedigitalcollection.asme.org/article.aspx?articleid=1434171.

[40] Tseng, P.-H., Tsai, K.-T., Chen, A.-L. & Wang, C.-C. Performance of novel liquid-cooled porous heat sink via 3-d laser additive manufacturing. *International Journal of Heat and Mass Transfer* **137**, 558–564 (2019). URL https://linkinghub.elsevier.com/retrieve/pii/S001793101834883X.

Statements and Declarations

Funding

The project was supported by the PERFORM program led by IRT Jules Verne.

Competing interest

The authors declare the following financial interests/personal relationships which may be considered as potential competing interests: the study was funded by the IRT

Jules Verne PERFORM program, fully acknowledged in the manuscript.

Author Contributions

All authors contributed to the design and development of the study. Material preparation, data collection and analysis were performed by Matthis Balthazar, Nicolas Baudin, Jérôme Soto and Vincent Sobotka. The first draft of the manuscript was written by Matthis Balthazar and all authors commented on previous versions of the manuscript. All authors read and approved the final manuscript.

Acknowledgment

The authors would like to acknowledge the funding of PERFORM project led by IRT Jules Verne. Authors wish to associate the industrial partners of PERFORM project. The authors would like to thank Nicolas Lefèvre and Gwenael Biotteau who helped for the experimental setups.